HHS Public Access

Author manuscript

J Mater Chem A Mater. Author manuscript; available in PMC 2018 September 28.

Published in final edited form as:

J Mater Chem A Mater. 2017 September 28; 5(36): 19485–19490. doi:10.1039/c7ta06338e.

Impact of fullerene derivative isomeric purity on the performance of inverted planar perovskite solar cells†

Edison Castro[a,iD], **Gerardo Zavala**[a], **Sairaman Seetharaman**[b], **Francis D'Souza**[iD,b], and **Luis Echegoyen**[iD,a]

[a]Department of Chemistry, University of Texas at El Pas, El Paso, TX, 79968, USA

[b]Department of Chemistry, University of North Texas, Denton, TX 76203-5017, USA

Abstract

The effect of utilizing a pure *cis*-α-dimethoxy carbonyl fulleropyrrolidine C_{70} ($DMEC_{70}$) isomer as the electron transporting material (ETM) in inverted perovskite solar cells (PSCs) was evaluated. The as-prepared C_{70} mono-adduct products are mixtures of regioisomers and the interest was to evaluate them independently as ETMs. Three different *cis*-$DMEC_{70}$ isomers (α, β-*endo* and β-*exo*) (mix-$DMEC_{70}$) were synthesized and purified by HPLC. It was found that PSCs based on the pure **α-$DMEC_{70}$** exhibit a substantially enhanced maximum power conversion efficiency (PCE) of 18.6% as compared to devices based on the mixed-$DMEC_{70}$ isomers that yielded a PCE of 16.4%. A maximum PCE of 15.7% was observed for devices based on [6,6]-phenyl-C_{71}-butyric acid methyl ester ($PC_{71}BM$). This work points out the importance of using pure fullerene derivative isomers as ETMs to reduce the intrinsic energy disorder, which enhances the overall device performance.

Introduction

Organic–inorganic halide PSCs offer great potential for cost-effective, solution-processable, and large-area fabrication of solar energy conversion technologies.[1,2] PSCs can be either fabricated using conventional n–i–p or inverted p–i–n configurations, and in both cases the perovskite layer is in contact with a hole transporting layer (HTL) and an electron transporting layer (ETL) on opposite sides. These selective interlayers not only improve the charge extraction from the perovskite layer but also determine the polarity of the device.[3,4] To date, PSCs present the fastest growth in terms of PCE with certified efficiencies rising from 3.8% in 2009 to 22.1% in 2016 for small-area devices (0.1 cm^2),[5,6] whereas a PCE of 19.6% has been reported for large-area devices (1 cm^2).[7] It is worth mentioning that higher

†Electronic supplementary information (ESI) available. See DOI: 10.1039/c7ta06338e

Correspondence to: Luis Echegoyen.

Edison Castro http://orcid.org/0000-0003-2954-9462
Francis D'Souza http://orcid.org/0000-0003-3815-8949
Luis Echegoyen http://orcid.org/0000-0003-1107-9423

Conflicts of interest

Authors declare no conflict of interest.

PCEs and long-term device stability have been achieved after the first report of an all-solid-state PSC, introduced by Kim *et al.* in 2009.[8]

In inverted PSCs, the HTL, typically PEDOT:PSS, modified PEDOT:PSS, or NiO_x,[9–14] is in contact with the anode (ITO or FTO), while the ETL, typically a fullerene derivative, is in contact with the back electrode (Al or Ag). The standard fullerenes used in PSCs are [6,6]-phenyl-$C_{61/71}$-butyric acid methyl esters ($PC_{61/71}BM$), mainly due to their efficient electron transporting and solution processable properties.[15,16] Inverted PSCs based on ITO/doped-poly[bis(4-phenyl)(2,4,6-trimethylphenyl)amine] (PTAA)/$MA_{0.60}FA_{0.40}PI_3$/$PC_{71}BM$/C_{60}/2,9-dimethyl-4,7-diphenyl-1,10-phenanthroline (BCP)/Ag have achieved a maximum PCE of 20.2%.[17]

Zhu[18] and Huang's[19] groups have reported that charge trap states at the surfaces and grain boundaries of perovskite crystals act as non-radiative recombination centers, which drastically affect the optoelectronic properties of PSCs. Snaith[20] and co-workers proposed that non-coordinated halide ions on the surface of perovskite crystals can be passivated using iodopenta fluorobenzene. The same group separately reported that crystal surface vacancies can be significantly passivated using organic Lewis bases such as thiophene and pyridine.[21] To mitigate the effects on grain boundaries and trap states, the concept of perovskite/fullerene (P/F) heterojunctions has attracted considerable attention.[22–25] Huang *et al.*[26] demonstrated that the trap states on the surface and grain boundaries are the origin of photocurrent hysteresis and that fullerene layers deposited on perovskites can effectively passivate these charge trap states and eliminate the undesirable photocurrent hysteresis.[26]

We have recently reported that PSCs based on an isomeric mixture (mix-$DMEC_{70}$) exhibited both higher PCE and higher device-stability than devices based on $PC_{71}BM$. These results were attributed to the ability of the mix-$DMEC_{70}$ to extract electrons efficiently, likely due to specific interactions between the pyrrolidine groups (carbonyls and amino groups) and the perovskite crystals at the interfaces.[27] There are three regioisomers in mix-$DMEC_{70}$ (*cis*-α, *cis*-β-*endo* and *cis*-β-*exo*) as shown in Fig. 1a. It should be noted that the as-prepared mix-$DMEC_{70}$ was used as the ETL in PSCs without further purification. The effect of using pure fullerene C_{60} bis-adduct isomers as opposed to isomeric mixtures in bulk heterojunction solar cells (BHJ-SCs) was first studied by Imahori *I*.[28] Pure isomers have been shown to have a smaller energy disorder and a higher electron mobility than their corresponding regioisomeric mixtures, thus leading to higher performance solar cells.[29–36] Imahori *et al.*[37] reported photophysical properties and remarkable photovoltaic performance improvement when using isomerically pure C_{70} mono-adducts in BHJ-SCs. Recently Huang *et al.*[38] reported the use of pure C_{60} bis-adducts in PSCs to match the energy levels to obtain higher photovoltaic performance.

Shao *et al.*[26] reported a simple solvent annealing method to mitigate the energy disorder in the $PC_{61}BM$ layer in PSCs, resulting in an improved open circuit voltage (V_{oc}). Grätzel *et al.*[39] recently reported that improved device performance and stability in PSCs can be obtained when using a pure bis-adduct of $PC_{61}BM$ as an additive in an antisolvent chlorobenzene solution. Since the packing of the C_{70} fullerene derivatives in the solid state should have an impact on their charge separation and transporting properties in PSCs, the

three obtained isomers were purified and characterized in this work, but only the pure **α-DMEC$_{70}$** was evaluated as the ETM in inverted PSCs since this compound was the major regioisomer obtained.

Results and discussion

By changing the reaction conditions from sonication at room temperature to reflux, the formation ratio of the **α-DMEC$_{70}$** with respect to the other two isomers (Fig. 1a) was improved from 82% to 90% (Scheme S1†). The detailed synthetic procedures and characterization are described in the ESI.† The pure *cis*-DMEC$_{70}$ isomers were purified by HPLC from the as-obtained mix-DMEC$_{70}$ using a 5PYE column. As shown in Fig. S1,† three peaks that correspond to the three DMEC$_{70}$ isomers were observed. The three different isomers were fully characterized by means of MALDI-TOF, 1D and 2D ^{1}H and ^{13}C-NMR, and UV-vis absorption (Fig. S2–S7†).

Fig. S5 and S6† show the UV-vis absorption profiles of the three DMEC$_{70}$ isomers in chloroform and the structures of the isomers were unambiguously assigned by comparing their UV-vis profiles with those of known C$_{70}$ fullerene analogs.[40]

The electrochemical properties of the three DMEC$_{70}$ isomers were measured using cyclic voltammetry (CV) (Fig. S8†). The DMEC$_{70}$ isomers exhibit three reduction waves in the negative potential range from 0 to −2.0 V *vs.* Fc/Fc^{+}. The lowest unoccupied molecular orbital (LUMO) energy levels were estimated from their onset reduction potentials (E_{red}^{on}),[41] and the corresponding values are listed in Table 1. The LUMO energy levels of *cis*-α, *cis*-β-*endo* and *cis*-β-*exo* were estimated to be −4.24 eV, −3.96 eV and −3.93 eV, respectively. These results show that the electrochemical properties of C$_{70}$ fullerene mono-adducts are affected by changing the position of the addend. The energylevel diagram of **α-DMEC$_{70}$** and mix-DMEC$_{70}$ is shown in Fig. 1b.

The electron mobilities of **α-DMEC$_{70}$**, mix-DMEC$_{70}$ and PC$_{71}$BM based on electron-only devices (ITO/Al/fullerene/Al) were calculated by the space-charge limited current (SCLC) method and the Mott–Gurney law,[42–45] and values of 9.98×10^{-4}, 8.01×10^{-4} and 9.20×10^{-4} cm^{2} V^{-1} s^{-1} were obtained, respectively.

As expected, the smaller energy disorder for the pure isomer leads to a higher electron mobility compared to the regioisomeric mixture (Fig. S9†).

To further characterize the effect of pure **α-DMEC$_{70}$** in PSCs, inverted planar PSCs using this compound as the ETM with a configuration of ITO/PEDOT:PSS/$CH_3NH_3PbI_3$/**α-DMEC$_{70}$**/Al were fabricated (see the Experimental section). Scanning electron microscopy (SEM) (Fig. 1c) of the perovskite surface shows a uniform microscale grain structure (~300 nm) with no apparent pinholes. Additionally, the cross section shown in Fig. 1d shows all of the different layers. The perovskite layer was also analyzed by X-ray diffraction (XRD). Fig. S10† shows diffraction peaks for a pure perovskite material with no evidence of PbI_2 or CH_3NH_2I.

The current density–voltage (J–V) curves of the inverted planar structures based on **α-DMEC$_{70}$**, mix-DMEC$_{70}$ and PC$_{71}$BM are shown in Fig. 2a. The photovoltaic parameters are listed in Table 2. As shown in Fig. 2a and in Table 2, the pure **α-DMEC$_{70}$** regioisomer based devices exhibit higher PCEs (18.6%) than those of mix-DMEC$_{70}$ and PC$_{71}$BM (16.4% and 15.6%, respectively).

As shown in Table 2, the V_{oc} values obtained from the **α-DMEC$_{70}$** based devices are higher than those obtained from the mix-DMEC$_{70}$ based devices. These results may seem counterintuitive solely based on HOMO–LUMO values, but recent results have demonstrated that the ETM layer order can affect and even reverse the expected results based on energy level considerations.[26] EQE spectra in Fig. 2b show that the charge extraction efficiency of the **α-DMEC$_{70}$**-based devices is higher than those the mix-DMEC$_{70}$ and PC$_{71}$BM-based devices.

The photocurrent density (J_{sc}) calculated from the EQE spectra agrees with the measured J_{sc} from the J–V curves, con-firming the accuracy of the device efficiency. The higher J_{sc} and FF obtained for the **α-DMEC$_{70}$**-based devices can be associated with the higher electron mobility of **α-DMEC$_{70}$**. The maximum steady-state photocurrent and PCE outputs were monitored by applying a voltage close to the maximum power and plotted as a function of time.

Fig. 2c shows that for devices based on **α-DMEC$_{70}$**, mix-DMEC$_{70}$ and PC$_{71}$BM steady-state photocurrents of 21.31 mA cm^{-2}, 19.81 mA cm^{-2}, and 18.11 mA cm^{-2} and PCEs of 18.3%, 15.8%, and 14.5% were obtained, respectively. The stabilized power outputs were calculated by multiplying the photocurrent and the applied voltage.

The statistical histograms of PCEs for 20 individual devices are shown in Fig. 2d. The distributions show average efficiencies of 17.9 ± 0.7%, 15.9 ± 0.5% and 14.8 ± 0.8% for **α-DMEC$_{70}$**, mix-DMEC$_{70}$ and PC$_{71}$BM based devices, respectively. To investigate the hysteresis behavior, the devices were tested in both forward and reverse scan directions.

As shown in Fig. 3a, all the devices displayed relatively consistent J–V curves regardless of the scan direction, indicating negligible hysteretic effects in the PSCs.

To study the charge carrier recombination of the devices based on DMEC$_{70}$ (pure and mixture) and PC$_{71}$BM as the ETMs, steady-state photoluminescence (PL) (Fig. 3b) and time-resolved PL decay measurements (Fig. 3c) were recorded for perovskite, perovskite/DMEC$_{70}$ (pure and mixture), and perovskite/PC$_{71}$BM films. As shown in Fig. 3b the emission peak at 778 nm is attributed to the recombination process in the nanocrystalline perovskite.

A significant PL quenching effect was observed within the perovskite/ETM thin films, which indicates that surface charge carrier recombination was suppressed.[46] Moreover, a more pronounced PL quenching effect was observed within the perovskite/**α-DMEC$_{70}$** thin film than for the perovskite/mix-DMEC$_{70}$ or perovskite/PC$_{71}$BM thin films, which resulted in an enhanced J_{sc} and FF, and thus in a higher PCE. Fig. 3c shows shorter PL decay times for perovskite/ETMs (0.10, 0.04 and 0.15 ns for perovskite/**α-DMEC$_{70}$**, perovskite/mix-

$DMEC_{70}$, and perovskite/$PC_{71}BM$, respectively) than for simple perovskite (0.21 ns) thin films.

The shortened decay lifetimes of the perovskite with any of the ETMs leads to faster transport of charge carriers and more efficient charge carrier collection, which suppresses electron–hole recombination and thus increases the J_{sc} and the FF.[47]

Air-stability is one of the major concerns for the commercialization of PSCs.[48,49] As shown in Fig. 3d, the stability of unencapsulated devices based on **α-DMEC$_{70}$**, mix-$DMEC_{70}$, and $PC_{71}BM$ as the ETMs was monitored for 10 days at room temperature with a relative humidity of ~20%. High stability was observed for the devices based on **α-DMEC$_{70}$**, which retained more than 60% of their initial PCE. In contrast, the mix-$DMEC_{70}$-based devices only retained 35% of their initial PCE, whereas the $PC_{71}BM$-based devices retained less than 10% of their initial PCE after 10 days. To understand the reasons for these differences, the contact angles of water droplets on perovskite/**α-DMEC$_{70}$**, perovskite/mix-$DMEC_{70}$ and perovskite/$PC_{71}BM$ were measured and the values were 92°, 86° and 82°, respectively (Fig. S11†). These small but significant differences clearly show that the improved stability of the **α-DMEC$_{70}$**-based devices can be attributed to the better packing of the pure isomer, which leads to a more hydrophobic and compact layer and thus reduces water intrusion into the perovskite layer.

The surface morphologies of perovskite, perovskite/mix-$DMEC_{70}$ and perovskite/**α-DMEC$_{70}$** films were characterized by atomic force microscopy (AFM). As shown in Fig. S12a,† the perovskite film exhibits a crystalline structure with a calculated root-mean-square (RMS) roughness of around 48 nm. The perovskite/mix-$DMEC_{70}$ film shows a morphology with a reduced RMS roughness of around 15.9 nm (Fig. S12b†), whereas a smoother morphology with a smaller RMS roughness of around 8.5 nm was observed for the perovskite/**α-DMEC$_{70}$** film (Fig. S12c†). The pure-isomer film leads to a smoother ETL, likely due to better molecular packing.

Conclusions

By changing the reaction conditions, we improved the yield of the **α-DMEC$_{70}$** isomer. Using this pure isomer as the ETM layer in PSCs resulted in considerably improved device performance and long-term stabilities. These improvements are likely the result of structural and energy advantages of using the single isomer and of improved hydrophobicity. To our knowledge, this is the first example of such an improvement observed by using a pure C_{70}-fullerene isomer, and the stabilized PCE of 18.3% is among the highest for this simple inverted PSC architecture. Our results highlight the importance of developing synthetic approaches that yield pure C_{70}-fullerene isomers without the need for HPLC purification.

Experimental section

Synthesis of $DMEC_{70}$

By changing the reaction conditions from sonication at room temperature to reflux, the formation ratio of the **α-DMEC$_{70}$** with respect to the other two isomers (Fig. 1a) was

improved from 82% to 90% (Scheme S1†). C_{70} (84 mg, 0.10 mmol) was dissolved in chlorobenzene (30 mL) under sonication for 5 min, and then DIB (200 mg, 0.62mmol), glycine methyl ester hydrochloride (100 mg, 0.79 mmol) and sodium carbonate decahydrate (100 mg, 0.35 mmol) were added. The flask was wrapped with aluminum foil and refluxed for 30 min. The solution was directly poured onto a silica gel column and CS_2 was used to separate the unreacted C_{70}, and $DMEC_{70}$ was purified using a toluene/ethyl acetate (9 : 1) mixture. The regioisomeric yield was 85%. The ratio of the mono-adducts in the mixture was 90 : 5 : 5 (α : β-*endo* : β-*exo*) as determined by ^{1}H NMR and the molecular mass was determined by matrix assisted laser desorption/ionization-time-of-light-mass spectrometry (MALDI-TOF-MS) (Fig. S1†).

Device fabrication

Methylammonium iodide (CH_3NH_3I) was prepared using a previously reported procedure.[50] PSCs with a configuration of ITO/PEDOT:PSS/perovskite/fullerene derivative/Al were fabricated on ITO-coated glass substrates with a resistivity of 10 Ω cm^{-2}. The patterned ITO glass substrates were cleaned sequentially with detergent, deionized water, isopropyl alcohol and acetone, each step for 30 min, and then dried with nitrogen gas and finally treated in a UV-ozone oven for 30 min. After passing through a 0.45 μm PVDF filter, the PEDOT:PSS solution (Baytron P VP AI 4083) was spin-coated onto the treated ITO substrates at 5000 rpm for 30 s, and heated at 150 °C for 15 min in air. Then the substrates were transferred to a N_2-filled glovebox where CH_3-NH_3PbI_3 (1 M solution in DMF) was spincoated on top of the PEDOT:PSS coated substrates at 800 rpm for 10 s and at 4000 rpm for 25 s, 80 μL of toluene were added 5 s after the second step and then the devices were annealed at 70 °C for 60 min and the fullerene derivatives dissolved in chlorobenzene (20 mg mL^{-1}) were spin-coated onto the CH_3-NH_3PbI_3 layer at 5000 rpm for 30 s. Finally, aluminum electrodes (100 nm) were deposited by thermal evaporation under a pressure of 1×10^{-6} Torr through a shadow mask. The active area of the fabricated devices was 6 mm^2. The top aluminum electrodes were encapsulated with a UV-curable epoxy resin and a glass slide before testing.

Supplementary Material

Refer to Web version on PubMed Central for supplementary material.

Acknowledgments

The authors thank the US National Science Foundation (NSF) for generous support of this work under the NSF-PREM program (DMR 1205302), CHE-1408865 (to L.E.) and 1401188 (to F. D.). The Robert A. Welch Foundation is also gratefully acknowledged for an endowed chair to L. E. (Grant AH-0033). The National Institute of General medical Sciences of the National Institutes of Health under linked Award Numbers RL5GM118969, TL4GM118971, and UL1GM118970, is also acknowledged.

References

1. Zhang H, Cheng J, Li D, Lin F, Mao J, Liang C, Jen AKY, Grätzel M, Choy WCH. Adv. Mater. 2017:1604695.
2. Shin SS, Yeom EJ, Yang WS, Hur S, Kim MG, Im J, Seo J, Noh JH, Seok SI. Science. 2017; 356:167–171. [PubMed: 28360134]
3. Ratcliff EL, Zacher B, Armstrong NR. J Phys. Chem. Lett. 2011; 2:1337–1350. [PubMed: 26295432]

4. Yang S, Fu W, Zhang Z, Chen H, Li C-Z. J Mater. Chem. A. 2017; 5:11462–11482.
5. Kojima A, Teshima K, Shirai Y, Miyasaka T. J Am. Chem. Soc. 2009; 131:6050–6051. [PubMed: 19366264]
6. NREL. [accessed June 2017] Best Research-Cell Efficiencies. Jun, 2017 http://www.nrel.gov/pv/assets/images/efficiency_chart.jpg
7. Li X, Bi D, Yi C, Décoppet J-D, Luo J, Zakeeruddin SM, Hagfeldt A, Grätzel M. Science. 2016; 353:58–62. [PubMed: 27284168]
8. Kim H-S, Lee C-R, Im J-H, Lee K-B, Moehl T, Marchioro A, Moon S-J, Humphry-Baker R, Yum J-H, Moser JE, Grätzel M, Park N-G. Sci. Rep. 2012; 2:591. [PubMed: 22912919]
9. Docampo P, Ball JM, Darwich M, Eperon GE, Snaith HJ. Nat. Commun. 2013; 4:2761. [PubMed: 24217714]
10. Jeng J-Y, Chen K-C, Chiang T-Y, Lin P-Y, Tsai T-D, Chang Y-C, Guo T-F, Chen P, Wen T-C, Hsu Y-J. Adv. Mater. 2014; 26:4107–4113. [PubMed: 24687334]
11. Wang J-M, Wang Z-K, Li M, Hu K-H, Yang Y-G, Hu Y, Gao X-Y, Liao L-S. ACS Appl. Mater. Interfaces. 2017; 9:13240–13246. [PubMed: 28332402]
12. Wang Z-K, Gong X, Li M, Hu Y, Wang J-M, Ma H, Liao L-S. ACS Nano. 2016; 10:5479–5489. [PubMed: 27128850]
13. Lou Y-H, Li M, Wang Z-K. Appl. Phys. Lett. 2016; 108:053301.
14. Wang Z-K, Li M, Yuan D-X, Shi X-B, Ma H, Liao L-S. ACS Appl. Mater. Interfaces. 2015; 7:9645–9651. [PubMed: 25897754]
15. Volker SF, Collavini S, Delgado JL. ChemSusChem. 2015; 8:3012–3028. [PubMed: 26311591]
16. Meng L, You J, Guo TF, Yang Y. Acc. Chem. Res. 2016; 49:155–165. [PubMed: 26693663]
17. Luo D, Zhao L, Wu J, Hu Q, Zhang Y, Xu Z, Liu Y, Liu T, Chen K, Yang W, Zhang W, Zhu R, Gong Q. Adv. Mater. 2017; 29:1604758.
18. Wu X, Trinh MT, Niesner D, Zhu H, Norman Z, Owen JS, Yaffe O, Kudisch BJ, Zhu XY. J Am. Chem. Soc. 2015; 137:2089–2096. [PubMed: 25602495]
19. Shao Y, Fang Y, Li T, Wang Q, Dong Q, Deng Y, Yuan Y, Wei H, Wang M, Gruverman A, Shield J, Huang J. Energy Environ. Sci. 2016; 9:1752–1759.
20. Abate A, Saliba M, Hollman DJ, Stranks SD, Wojciechowski K, Avolio R, Grancini G, Petrozza A, Snaith HJ. Nano Lett. 2014; 14:3247–3254. [PubMed: 24787646]
21. Noel NK, Abate A, Stranks SD, Parrott ES, Burlakov VM, Goriely A, Snaith HJ. ACS Nano. 2014; 8:9815–9821. [PubMed: 25171692]
22. Xu J, Buin A, Ip AH, Li W, Voznyy O, Comin R, Yuan M, Jeon S, Ning Z, McDowell JJ, Kanjanaboos P, Sun J-P, Lan X, Quan LN, Kim DH, Hill IG, Maksymovych P, Sargent EH. Nat. Commun. 2015; 6:7081. [PubMed: 25953105]
23. Wang K, Liu C, Du P, Zheng J, Gong X. Energy Environ. Sci. 2015; 8:1245–1255.
24. Chiang C-H, Wu C-G. Nat. Photonics. 2016; 10:196–200.
25. Zhao Y, Zhou W, Ma W, Meng S, Li H, Wei J, Fu R, Liu K, Yu D, Zhao Q. ACS Energy Lett. 2016; 1:266–272.
26. Shao Y, Xiao Z, Bi C, Yuan Y, Huang J. Nat. Commun. 2014; 5:5784. [PubMed: 25503258]
27. Tian C, Castro E, Wang T, Betancourt-Solis G, Rodriguez G, Echegoyen L. ACS Appl. Mater. Interfaces. 2016; 8:31426–31432. [PubMed: 27766845]
28. Kitaura S, Kurotobi K, Sato M, Takano Y, Umeyama T, Imahori H. Chem. Commun. 2012; 48:8550–8552.
29. Meng X, Zhao G, Xu Q, Tan Za, Zhang Z, Jiang L, Shu C, Wang C, Li Y. Adv. Funct. Mater. 2014; 24:158–163.
30. Tao R, Umeyama T, Kurotobi K, Imahori H. ACS Appl. Mater. Interfaces. 2014; 6:17313–17322. [PubMed: 25208339]
31. Tao R, Umeyama T, Higashino T, Koganezawa T, Imahori H. ACS Appl. Mater. Interfaces. 2015; 7:16676–16685. [PubMed: 26177008]
32. Tao R, Umeyama T, Higashino T, Koganezawa T, Imahori H. Chem. Commun. 2015; 51:8233–8236.

33. Zhao F, Meng X, Feng Y, Jin Z, Zhou Q, Li H, Jiang L, Wang J, Li Y, Wang C. J Mater. Chem. A. 2015; 3:14991–14995.
34. Zhang B, Subbiah J, Jones DJ, Wong WWH. Beilstein J. Org. Chem. 2016; 12:903–911. [PubMed: 27340480]
35. Xiao Z, Geng X, He D, Jia X, Ding L. Energy Environ. Sci. 2016; 9:2114–2121.
36. Cao T, Chen N, Liu G, Wan Y, Perea JD, Xia Y, Wang Z, Song B, Li N, Li X, Zhou Y, Brabec CJ, Li Y. J Mater. Chem. A. 2017; 5:10206–10219.
37. Umeyama T, Miyata T, Jakowetz AC, Shibata S, Kurotobi K, Higashino T, Koganezawa T, Tsujimoto M, Gelinas S, Matsuda W, Seki S, Friend RH, Imahori H. Chem. Sci. 2017; 8:181–188. [PubMed: 28451164]
38. Lin Y, Chen B, Zhao F, Zheng X, Deng Y, Shao Y, Fang Y, Bai Y, Wang C, Huang J. Adv. Mater. 2017:1700607.
39. Zhang F, Shi W, Luo J, Pellet N, Yi C, Li X, Zhao X, Dennis TJS, Li X, Wang S, Xiao Y, Zakeeruddin SM, Bi D, Grätzel M. Adv. Mater. 2017:1606806.
40. Castro E, Martinez ZS, Seong CS, Cabrera-Espinoza A, Ruiz M, Hernandez AG, Valdez F, Llano M, Echegoyen LA. J Med. Chem. 2016; 59:10963–10973. [PubMed: 28002960]
41. Cardona CM, Li W, Kaifer AE, Stockdale D, Bazan GC. Adv. Mater. 2011; 23:2367–2371. [PubMed: 21462372]
42. Mihailetchi VD, Wildeman J, Blom PWM. Phys. Rev. Lett. 2005; 94:126602. [PubMed: 15903944]
43. Lou Y-H, Wang Z-K, Yuan D-X, Okada H, Liao L-S. Appl. Phys. Lett. 2014; 105:113301.
44. Wang Z, Lou Y, Naka S, Okada H. Appl. Phys. Lett. 2011; 98:063302.
45. Lou Y-H, Xu M-F, Zhang L, Wang Z-K, Naka S, Okada H, Liao L-S. Org. Electron. 2013; 14:2698–2704.
46. You J, Hong Z, Yang Y, Chen Q, Cai M, Song T-B, Chen C-C, Lu S, Liu Y, Zhou H. ACS Nano. 2014; 8:1674–1680. [PubMed: 24386933]
47. Liang P-W, Liao C-Y, Chueh C-C, Zuo F, Williams ST, Xin X-K, Lin J, Jen AKY. Adv. Mater. 2014; 26:3748–3754. [PubMed: 24634141]
48. Grätzel M. Nat. Mater. 2014; 13:838–842. [PubMed: 25141800]
49. Niu G, Guo X, Wang L. J Mater. Chem. A. 2015; 3:8970–8980.
50. Chen Q, Zhou H, Hong Z, Luo S, Duan H-S, Wang H-H, Liu Y, Li G, Yang Y. J Am. Chem. Soc. 2014; 136:622–625. [PubMed: 24359486]

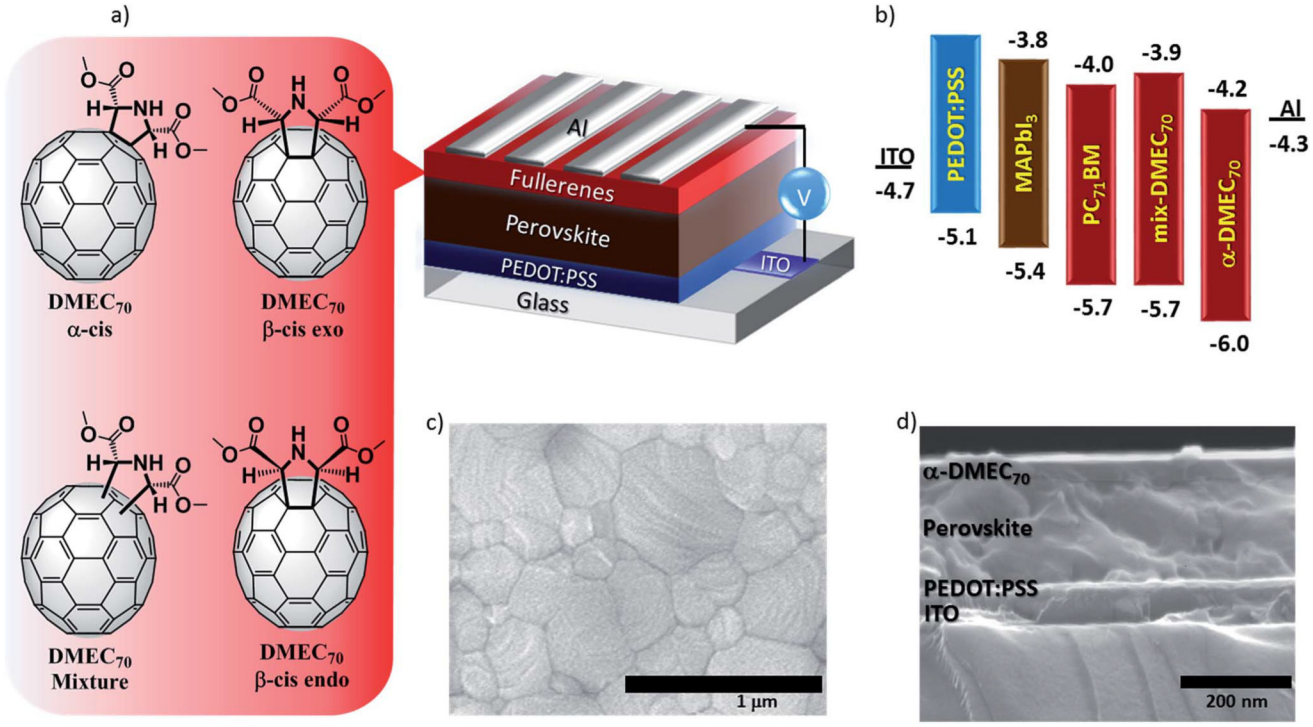

Fig. 1.

(a) Device structure of the inverted PSC using **α-DMEC$_{70}$**, mix-DMEC$_{70}$, or PC$_{71}$BM as the ETM. (b) Schematic illustration of the estimated HOMO and LUMO energy levels, calculated from CV and UV-vis. (c) Top-view SEM image of $CH_3NH_3PbI_3$ deposited on PEDOT:PSS. (d) Cross-sectional SEM image of an inverted PSC.

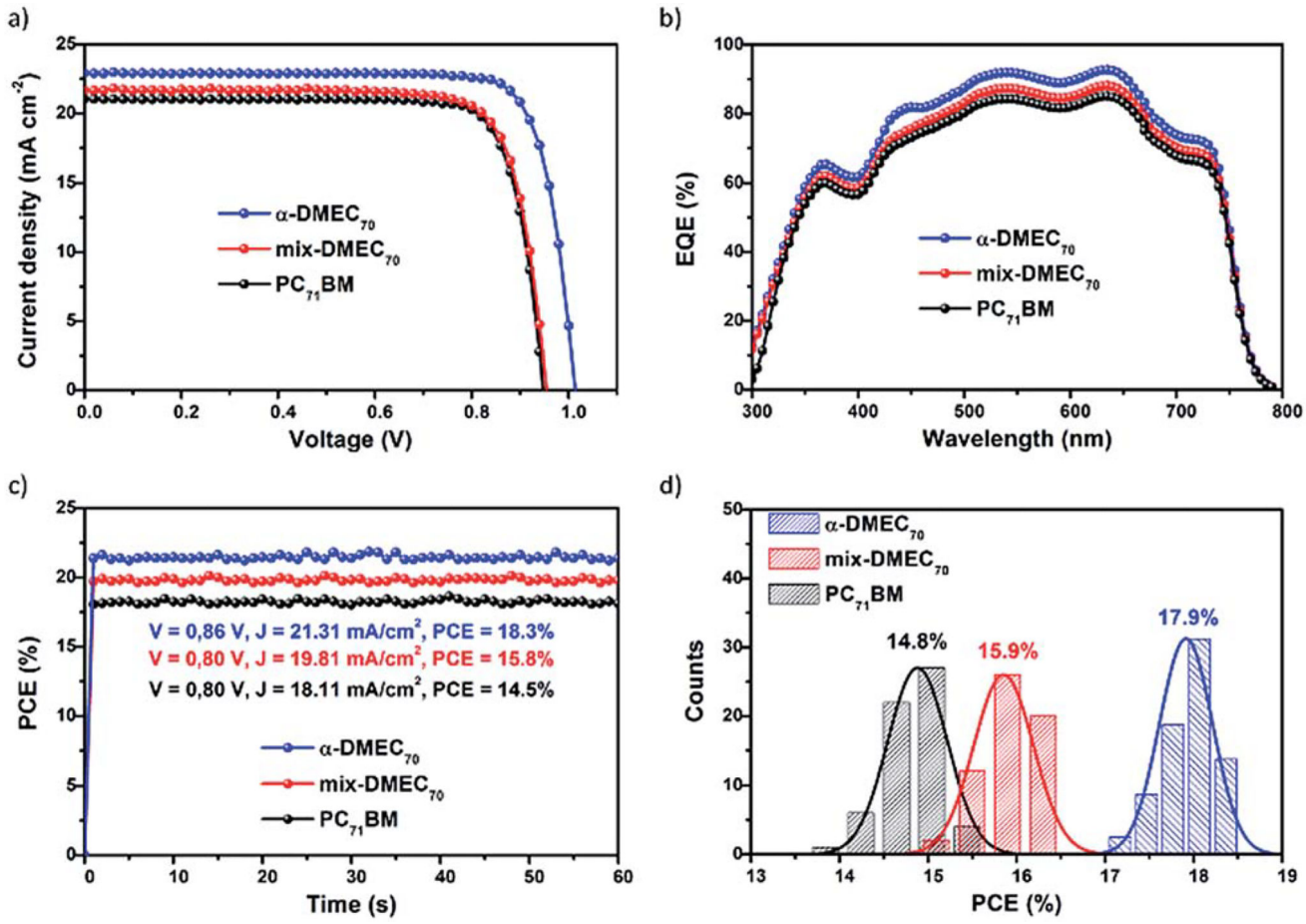

Fig. 2.

(a) *J–V* curves under 1 sun illumination. (b) EQE spectra of perovskite solar cells fabricated using **α-DMEC$_{70}$**, mix-DMEC$_{70}$ or PC$_{71}$BM as the ETM. (c) Power output under maximum power point tracking for 60 s. (d) The PCE histograms measured for 20 independent devices.

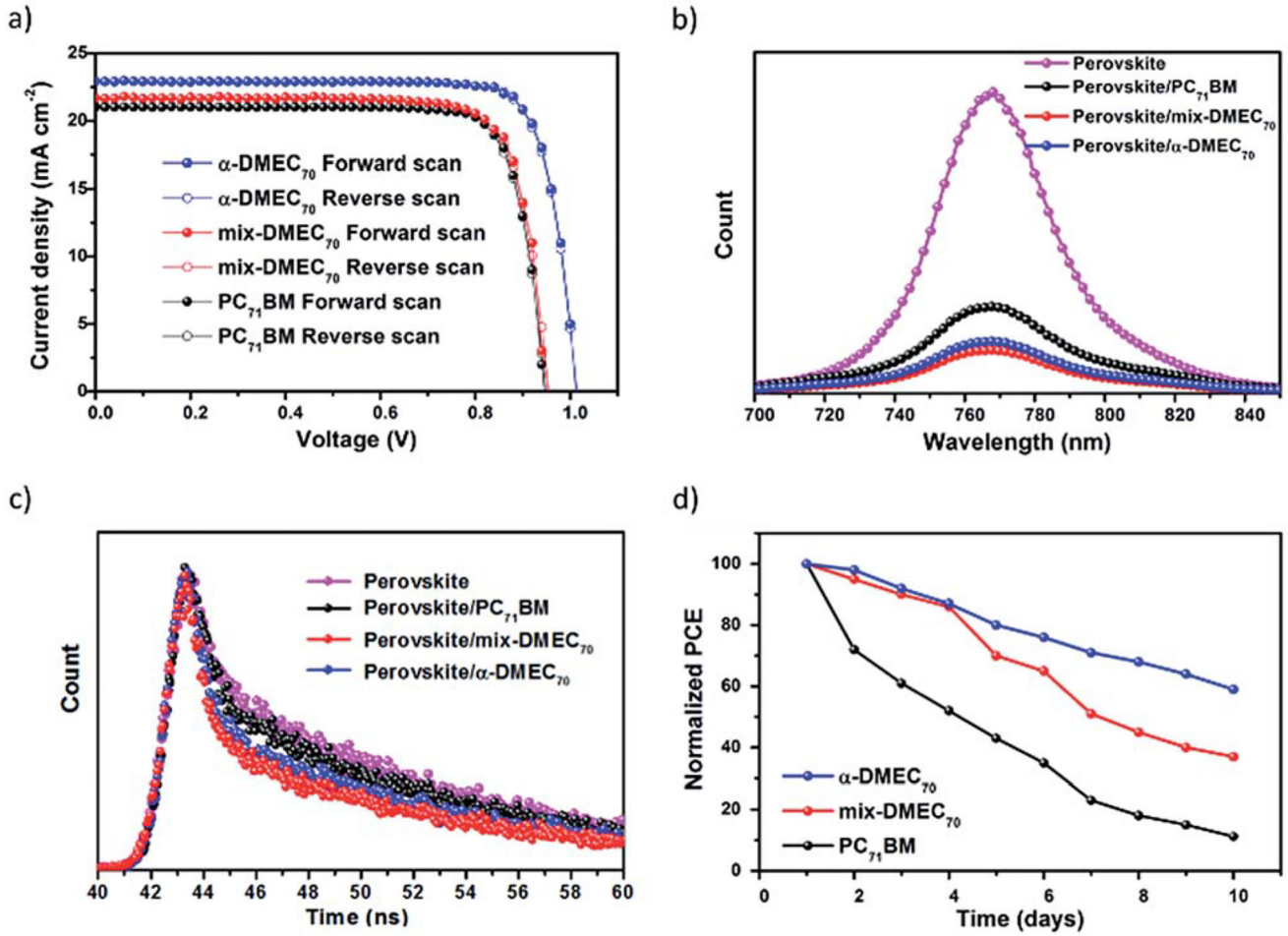

Fig. 3.

(a) *J–V* curves under 1 sun illumination in forward and reverse voltage scans. (b) Steady-state PL spectra of the perovskite and perovskite/ETM films. (c) TR-PL spectra of the perovskite and perovskite/ETM films. (d) Normalized PCE of PSCs measured as a function of time at ~20% humidity at room temperature.

Table 1

Electrochemical and photophysical data of **α**-DMEC$_{70}$, **β**-*endo*-DMEC$_{70}$ and **β**-*exo*-DMEC$_{70}$

Compound	λ_{abs} (nm)	E_g (eV)	E^{on}_{red}(V)	LUMO (eV)	HOMO (eV)
α-DMEC$_{70}$	683	1.81	−0.78	−4.24	−6.05
β-*endo*-DMEC$_{70}$	705	1.76	−1.06	−3.96	−5.72
β-*exo*-DMEC$_{70}$	705	1.76	−1.09	−3.93	−5.69

J Mater Chem A Mater. Author manuscript; available in PMC 2018 September 28.

Table 2

Summary of the performance of devices based on **α**-$DMEC_{70}$, mix-$DMEC_{70}$, or $PC_{71}BM$ as the ETM

ETM	J_{sc} (mA cm^{-2})[a]	J_{sc} (mA cm^{-2})	V_{oc} (V)	FF (%)	PCE (%)
α-$DMEC_{70}$	22.88	22.90	1.02	0.80	17.9 ± 0.7 (18.6)
mix-$DMEC_{70}$	21.90	21.92	0.95	0.77	15.9 ± 0.5 (16.4)
$PC_{71}BM$	21.07	21.09	0.95	0.78	14.8 ± 0.8 (15.6)

[a]Calculated current; () highest PCE. The average was calculated from 20 devices.